Neutron-diffraction study of $R\mathrm{NiO_3}$ (R = La,Pr,Nd,Sm): Electronically induced structural changes across the metal-insulator transition

J. L. García-Muñoz and J. Rodríguez-Carvajal
Institut Laue-Langevin, 156 X, 38042 Grenoble CEDEX, France

P. Lacorre
Laboratoire des Fluorures, Université du Maine, Avenue Olivier-Messiaen, 72017 Le Mans CEDEX, France and IBM Research Division, Almaden Research Center, 650 Harry Road, San Jose, California 95120-6099

J. B. Torrance
IBM Research Division, Almaden Research Center, 650 Harry Road, San Jose, California 95120-6099
(Received 10 October 1991; revised manuscript received 16 March 1992)

In the $R\mathrm{NiO_3}$ series (R = La,Pr,Nd,Sm), the metal-insulator (M-I) transition temperature rises systematically as the size of the rare earth decreases and as the subsequent distortion from the ideal cubic perovskite increases. For R = La the system keeps its metallic character down to 1.5 K, while for R = Pr, Nd, and Sm electronic localization occurs at 135, 200, and 400 K, respectively. High-resolution neutron-powder-diffraction experiments have been performed to investigate the structural anomalies across the first-order M-I transition in the orthorhombic $\mathrm{PrNiO_3}$ and $\mathrm{NdNiO_3}$ compounds. The cell volume undergoes a subtle increase when the compounds become insulating, due to a slight increase of the Ni-O distances. This effect is accompanied by coupled tilts of $\mathrm{NiO_6}$ octahedra, which imply changes in the Ni-O-Ni angles ($\Delta\Theta_{\mathrm{O\text{-}Ni\text{-}O}} \approx -0.5°$) governing the transfer integral between Ni e_g and O $2p$ orbitals. These changes are sterically driven by the observed increase of the nickel-oxygen distances ($\Delta d_{\mathrm{Ni\text{-}O}} \approx +0.004$ Å) in the insulating (low-temperature) phase. The results of valence-bond calculations suggest the existence of $\mathrm{Ni^{3+}}(d^7)$ and R^{3+} states for nickel and rare earth.

INTRODUCTION

The electronic structures of both simple and complex oxides of transition metals (TM's) have regained interest since the recent discovery of the high-T_c superconductors. It is worth remembering that these oxides belong to a more extensive group of TM compounds whose magnetic and transport properties have been controversial topics for the last 50 years.

Many TM compounds are known to exhibit metal-nonmetal transitions as a function of temperature or pressure. In most cases their mechanism is not yet well understood. Most of the theories presented to explain the lack of conductivity in the insulating TM oxides, sulfides, and halides can be extended to give a M-I transition. The strong correlation effects found in these materials are the reason for the breakdown of the one-electron picture, as presented in the theory of solids by Bloch[1] and Wilson.[2] Historically, the model of noninteracting electrons given by Wilson was followed by many other attempts, which can be divided into three nonisolated groups, depending on whether the insulating state is due to electron-electron interactions, antiferromagnetic correlations, or electron-phonon interactions. In order to understand the nature of band gaps, the origin of magnetism, and the conduction properties, it is essential to know the fundamental electronic energies that determine the broad spectrum of behaviors exhibited by these TM compounds.

Mott[3] and, later, Hubbard[4] broached the breakdown of the one-electron description by including the d-d Coulomb and exchange energies (U), involved in charge fluctuations of the type $d_i^n d_j^n \rightarrow d_i^{n-1} d_j^{n+1}$ (where i and j label sites and n the d-orbital occupation). For $U \gg W$ (W the conduction-band width) these charge fluctuations become of high energy compared with the spin-only excitations and are suppressed, justifying the use of spin-only Hamiltonians to describe the low-energy scale properties of magnetic insulators. These ideas were successfully applied to many systems (V, Ti, and Cr oxides and halides), especially to the early (Ti–Cr) TM compounds,[5] reproducing phase diagrams that included metallic, paramagnetic insulating, and antiferromagnetic insulating regions.

In 1985, Zaanen, Sawatzky, and Allen (ZSA) (Ref. 6) showed that for the late TM compounds (Mn→Cu) the Mott-Hubbard picture, in which the lowest-energy charge fluctuations excitations involve only d states, should be extended to also include charge-fluctuation energies that do not involve U, namely the charge transfer (Δ) $d_i^n \rightarrow d_j^{n+1}\underline{L}$, where $\underline{L}$ denotes a hole in the anion valance band. Both (U and Δ) are energies fundamental to our understanding of the undoped Cu- and Ni-oxide systems and underlie the assumptions of the different theories for the high-T_c superconductors.

The ZSA framework describes band gaps and electronic structures of TM compounds as a function of W (the one-electron dispersional bandwidth), the charge-transfer energy (Δ), the d-d Coulomb interaction (U), which also

includes exchange, and the hybridization interaction (T) described in the ligand-field theory. In this theory, insulating oxides (as well as halides, sulfides, etc.) are divided into charge-transfer insulators ($W<\Delta<U$) and Mott-Hubbard insulators ($W<U<\Delta$). The metallic region in the theoretical phase diagram includes two types, low-Δ metals ($\Delta<W$) and low-U metals ($U<W$), depending on the main character (p or d) of the band with which the lowest-lying metallic conduction band overlaps. A particularly simple procedure for estimating the values of U and Δ from ionization and Madelung potentials has been developed in Ref. 7.

Within the context of electronically correlated late TM systems, the perovskite-type compounds RNiO$_3$ (R stands for a rare earth) have been prepared,[8] but little work has been reported on their properties. One of the reasons lies in the difficulty of synthesizing these compounds, since they require elevated temperatures and high oxygen pressures.

Though not extensively investigated, LaNiO$_3$ is the best known among these nickelates. The compound is metallic over the whole temperature range and Pauli paramagnetic by virtue of strong Ni-O-Ni orbital overlap. Rhombohedrically distorted, it shows no evidence of a static Jahn-Teller distortion associated with the single e_g electron (if one admits the low spin Ni^{III} state for nickel: $t_{2g}^6 e_g^1$). This partially filled e_g orbital would be transformed into partially filled σ^* band states. There is no spontaneous magnetization of the conduction-band states. The Pauli susceptibility ($\chi_P \sim 9.09\times10^{-4}$ emu/mol) is anomalously high (over an order of magnitude greater than expected from a simple band model). It was studied by Goodenough *et al.*,[9] who interpreted its enhanced value and temperature dependence in the light of a highly correlated gas of ferromagnetically coupled spin polarons.

Recent spectroscopic work[10] provides evidence that the density of states near the Fermi level (E_F) is very low (much lower than expected from band calculations and from the Pauli susceptibility). This, together with a large effective mass, could be a consequence of the conduction-band width being not substantially greater than its critical value for the metallic state stability. A comparison with other TM oxides suggests[7] that LaNiO$_3$ falls on the boundary between metal and charge-transfer insulator.

Very recently[11] a metal-insulator (M-I) transition has been observed from resistivity measurements in the RNiO$_3$ series with R=Pr, Nd, and Sm, and neutron-diffraction experiments have shown small structural changes at the transition. The transition temperature ($T_{M\text{-}I}$) rises systematically as the lanthanide ionic size becomes smaller (i.e., as orthorhombic distortion increases). For Pr, Nd, and Sm nickelates the electronic localization occurs at 135, 200, and 400 K, respectively.

Another important fact concerning the electronic structure is the lack of knowledge about the real charge state of nickel in these oxides. The apparent evidence that doping or nonstoichiometry makes holes in the oxygen band (O^-) in several nickel and copper oxides[12–14] (as $Li_xNi_{1-x}O$ or $La_{2-x}Sr_xNiO_4$) implies reasonable doubts about the electronic state of nickel, that is, about the primary character of holes in RNiO$_3$ when the system is seen as the extreme of oxygen doped RNiO$_{2.5}$ ($R^{3+}Ni^{2+}O^{2-}_{2.5}$).

We have initiated an extensive experimental study (x-ray absorption, transport and magnetic measurements, polarized neutrons) on these compounds in order to get a deeper insight into the relevant phenomena determining the M-I transition. The results of these experiments will be published in subsequent papers. In the present work, we report the results of a high-resolution neutron-powder-diffraction study of PrNiO$_3$ and NdNiO$_3$ at room, low temperatures and on both sides of the M-I transition. These studies reveal the existence of structural anomalies associated with the change in the electronic state, and the detailed analysis of the structure gives important information about the electronic state of nickel in these systems. The compound LaNiO$_3$ has also been studied by neutron diffraction in order to have better structural parameters than those given in the literature. However, in this paper, only selected geometrical values are used for comparison purposes. Also, the thermal evolution of the cell parameters of SmNiO$_3$ across its M-I transition at 400 K has been studied by high-temperature x-ray diffraction.

EXPERIMENT

Sample preparation

The RNiO$_3$ (R=Pr,Nd,Sm) polycrystalline samples were synthesized according to the procedure described in Ref. 11. The resulting samples were dark brown to black in color. LaNiO$_3$ was prepared at 850 °C in 1 atm of flowing oxygen.

Neutron diffraction

Several neutron-diffraction experiments were carried out at the High Flux Reactor of the Institut Laue Langevin (Grenoble). Three samples prepared with the methods described above were used: LaNiO$_3$, PrNiO$_3$, and NdNiO$_3$.

Neutron experiments were performed in the medium-resolution D1B diffractometer (λ=2.52 Å) and the high-resolution powder diffractometer D2B (λ=1.594 Å). For the low-temperature range, a vanadium can with the sample inside was placed in a helium cryostat. The temperature stability was approximately ±0.1 K. Both diffractometers are equipped with multidetectors spanning an angular range of 80 and 160 degrees (2θ), respectively. The D1B experimental conditions are given in Ref. 11. Diffraction patterns on D2B were recorded at the following temperatures: 1.5, 30, 100, and 293 K for LaNiO$_3$; 1.5, 110, 145, and 293 K for PrNiO$_3$; and 1.5, 170, 190, 215, and 293 K for NdNiO$_3$. The total measuring time for each sample and temperature ranged from 3 to 4 h.

X-ray diffraction

Because of the very high absorption coefficient of Sm for neutrons, the structural changes at the M-I transition

at 400 K of $SmNiO_3$ were studied by means of high-temperature x-ray diffraction. A Siemens D5000 powder diffractometer (Co $K\alpha$ radiation) equipped with a position-sensitive detector was used. The sample was placed inside a protective chamber, on a horizontal platinum plate used both as sample holder and heating resistance. Data over a 20°–140° 2θ range were obtained at 20 different temperature settings between 278 and 483 K. The temperature stability was ~1 K. Three diffraction patterns, each of them with a measuring time of 30 min, were collected at each temperature, then summed before data analysis.

Data analysis

All the data were analyzed by the Rietveld method by using the programs available in the STRAP package.[15] A very small amount of NiO was detected and included as a second phase. Single and automatic sequential refinements were performed. Patterns on D2B were analyzed by interpolating the background between selected points or by refinement of a six-parameter polynomial function. For the cyclic refinements (D1B data) the background was refined using three free parameters. A previous account of the D1B experimental results was given in Ref. 11.

The data obtained on D2B were carefully analyzed in order to thoroughly study the details of the structure (mainly oxygen positions and distances) because relatively small changes were expected. Special care was taken to detect any dependence of the parameter values at convergence on changes in the starting point. The shapes of the Bragg peaks were fitted with a pseudo-Voigt function.

RESULTS AND DISCUSSION

Crystal structure of $LaNiO_3$ down to 1.5 K

Although the structure of $LaNiO_3$ is relatively well known at RT, the lack of neutron-diffraction data led us to complete our study with some high-resolution measurements on this metallic and rhombohedral compound. As was shown by Wold, Post, and Banks,[16] the rhombohedral distortion has $R\bar{3}c$ symmetry, which arises from a rotation of the NiO_6 octahedra about the threefold axis of the ideal cubic perovskite. The structural parameters, referred to the hexagonal axes, at four temperatures down to 1.5 K are displayed in Table I. Cell parameters are in good agreement with those reported in Refs. 16 and 17. They exhibit a smooth evolution from RT down to 1.5 K, consisting of a continuous but very slight increase in the rhombohedral distortion as the temperature is reduced.

Room-temperature crystal structures of $PrNiO_3$ and $NdNiO_3$

As been previously reported,[8,11] $PrNiO_3$ and $NdNiO_3$ have orthorhombic $GdFeO_3$-type structures up to high temperatures[17] (see Fig. 1). At RT the space group is *Pbnm*, which is the most common in perovskites with orthorhombic distortion.[18] From differential thermal analysis (DTA), the transition to rhombohedral symmetry ($R\bar{3}c$) takes place at ≈500 °C in $PrNiO_3$ and ≈920 °C in $NdNiO_3$.

The refined atomic positions, lattice parameters, and isotropic temperature factors B for all atoms, together with reliability factors, are listed in Table II. Tables III and IV show the main distances and angles, calculated from the refined atomic coordinates. These results are generally in good agreement with those previously reported from independent x-ray and neutron-diffraction data.[11,17] Selected observed and calculated patterns are shown in Fig. 2.

The oxygen content was verified by refining the occupation factors of the oxygen sites in all samples. The stoichiometry was found to be exactly the nominal, within the calculated standard errors (0.5% for oxygen

TABLE I. Structural parameters for metallic and rhombohedral ($R\bar{3}c$) $LaNiO_3$. (The structure is referred to the hexagonal axes.) La occupies the site (6a) (0 0 $\frac{1}{4}$), the Ni atom is at (6b) (0 0 0), and oxygen is at (18e) (x 0 $\frac{1}{4}$).

	$LaNiO_3$			
Temperature	1.5 K	30 K	100 K	RT
La B (Å^2)	0.06(2)	0.07(2)	0.12(2)	0.36(2)
Ni B (Å^2)	0.08(2)	0.07(2)	0.09(2)	0.21(2)
O x	0.5468(1)	0.5468(1)	0.5467(1)	0.5456(2)
B (Å^2)	0.23(2)	0.22(2)	0.27(2)	0.55(2)
Cell parameters				
a (Å)	5.4535(1)	5.4535(1)	5.4536(1)	5.4573(1)
c (Å)	13.1010(3)	13.1014(3)	13.1062(3)	13.1462(3)
Reliability factors (%)				
χ^2	5.5	3.9	3.9	3.5
R_B	4.1	4.3	4.1	4.5
$d_{Ni\text{-}O}$ (Å)	1.933(1)	1.933(1)	1.933(1)	1.935(1)
∠Ni-O-Ni (deg)	164.8(1)	164.8(1)	164.9(1)	165.2(1)

TABLE II. Structural parameters for $PrNiO_3$ and $NdNiO_3$ from refined D2B data. Rare-earth atom and O(1) are at (4c) (x y $\frac{1}{4}$), Ni is at (4b) ($\frac{1}{2}$ 0 0), and O(2) is in general (8d) (x y z) position.

	$PrNiO_3$					$NdNiO_3$			
Temperature	1.5 K	110 K	145 K	RT		1.5 K	170 K	215 K	RT
Space Group	*Pbnm*	*Pbnm*	*Pbnm*	*Pbnm*		*Pbnm*	*Pbnm*	*Pbnm*	*Pbnm*
				Atom coordinates and isotropic temperature factors					
Pr x	0.9939(5)	0.9950(7)	0.9945(6)	0.9944(6)	Nd x	0.994(1)	0.9932(8)	0.9972(13)	0.9941(8)
y	0.0329(4)	0.0325(4)	0.0305(4)	0.0286(5)	y	0.0384(3)	0.0374(3)	0.0360(5)	0.0343(3)
B (Å^2)	0.41(3)	0.46(3)	0.52(3)	0.66(3)	B (Å^2)	0.22(3)	0.38(3)	0.64(4)	0.61(3)
Ni B (Å^2)	0.36(1)	0.41(1)	0.43(1)	0.50(1)	Ni B (Å^2)	0.43(2)	0.48(1)	0.64(3)	0.51(1)
O(1) x	0.0704(3)	0.0697(4)	0.0681(3)	0.0665(4)	O(1) x	0.0731(13)	0.0711(11)	0.0710(14)	0.070(1)
y	0.4925(4)	0.4936(2)	0.4935(4)	0.4952(5)	y	0.4919(7)	0.4917(6)	0.4903(9)	0.4921(7)
B (Å^2)	0.49(2)	0.59(3)	0.60(3)	0.71(3)	B (Å^2)	0.38(5)	0.55(4)	0.45(7)	0.76(5)
O(2) x	0.7181(2)	0.7170(2)	0.7190(2)	0.7197(2)	O(2) x	0.7116(8)	0.7139(6)	0.7120(9)	0.7150(6)
y	0.2820(2)	0.2826(3)	0.2814(3)	0.2808(2)	y	0.2866(8)	0.2877(6)	0.2850(10)	0.2842(6)
z	0.0372(2)	0.0364(2)	0.0356(2)	0.0357(2)	z	0.0387(5)	0.0390(4)	0.0366(6)	0.0378(4)
B (Å^2)	0.67(2)	0.70(2)	0.72(2)	0.83(2)	B (Å^2)	0.85(4)	0.86(3)	1.03(5)	0.88(4)
				Cell parameters					
a (Å)	5.4155(1)	5.4133(1)	5.4115(1)	5.4193(1)	a (Å)	5.3824(3)	5.3836(2)	5.3879(4)	5.3891(3)
b (Å)	5.3884(1)	5.3828(1)	5.3763(1)	5.3801(1)	b (Å)	5.3861(2)	5.3863(2)	5.3797(3)	5.3816(2)
c (Å)	7.6164(1)	7.6227(1)	7.6163(1)	7.6263(1)	c (Å)	7.6066(3)	7.6078(3)	7.6058(4)	7.6101(3)
				Reliability factors (%)					
R_{WP}	6.0	5.7	5.8	5.8	R_{WP}	6.6	6.4	8.1	6.0
R_{expt}	3.6	3.6	3.7	3.5	R_{expt}	4.2	3.7	6.8	2.9
χ^2	2.8	2.5	2.5	2.7	χ^2	2.5	3.0	1.4	4.5
R_B	3.9	4.3	4.8	3.5	R_B	6.2	3.7	7.1	4.2

TABLE III. Interatomic distances (Å) and angles (°) for the Ni-O octahedron. (Δ_d in the table is defined as $\Delta_d=(1/N)\sum_{i=1}^{N}[(R_i-\langle R\rangle)/\langle R\rangle]^2$.)

	$PrNiO_3$					$NdNiO_3$				
		Temperature					Temperature			
	No.	1.5 K	110 K	145 K	RT	No.	1.5 K	170 K	215 K	RT
$d_{Ni\text{-}O(1)}$	2	1.942(1)	1.943(1)	1.939(1)	1.940(1)	$d_{Ni\text{-}O(1)}$	2	1.942(2)	1.941(2)	1.940(2)	1.940(2)
$d_{Ni\text{-}O(2)}$	2	1.944(1)	1.942(1)	1.941(1)	1.943(1)	$d_{Ni\text{-}O(2)}$	2	1.941(4)	1.953(3)	1.932(5)	1.940(3)
	2	1.946(1)	1.948(1)	1.941(1)	1.942(1)		2	1.954(4)	1.941(3)	1.955(5)	1.947(3)
$\langle d_{Ni\text{-}O}\rangle$		1.944(1)	1.944(1)	1.940(1)	1.942(1)	$\langle d_{Ni\text{-}O}\rangle$		1.946(3)	1.945(3)	1.942(4)	1.942(3)
$10^4\Delta_d$		0.008	0.015	0.000	0.001	$10^4\Delta_d$		0.087	0.092	0.244	0.030
∠O(1)-Ni-O(2)	2	89.6(1)	89.5(1)	89.6(1)	89.2(1)	∠O(1)-Ni-O(2)	2	89.3(3)	89.2(3)	89.8(3)	89.3(3)
	2	89.9(1)	90.1(1)	90.0(1)	90.0(1)		2	90.0(3)	89.6(3)	90.1(3)	89.7(3)
	2	90.1(1)	89.9(1)	89.9(1)	89.9(1)		2	90.0(3)	90.4(2)	89.9(3)	90.3(2)
	2	90.4(1)	90.5(1)	90.4(1)	90.8(1)		2	90.7(3)	90.8(2)	90.2(3)	90.7(2)
∠O(2)-Ni-O(2)	2	88.5(1)	88.5(1)	88.5(1)	88.5(1)	∠O(2)-Ni-O(2)	2	88.8(3)	88.6(2)	88.8(4)	88.7(2)
	2	91.5(1)	91.5(1)	91.5(1)	91.5(1)		2	91.2(3)	91.4(2)	91.2(4)	91.3(2)
∠Ni-O(1)-Ni	2	157.2(1)	157.5(1)	158.0(1)	158.5(1)	∠Ni-O(1)-Ni	2	156.5(3)	157.1(2)	157.0(3)	157.6(3)
∠Ni-O(2)-Ni	4	157.8(2)	157.8(3)	158.6(3)	158.7(2)	∠Ni-O(2)-Ni	4	155.7(8)	155.7(6)	156.7(9)	156.8(7)
⟨∠Ni-O-Ni⟩		157.6(1)	157.7(1)	158.3(1)	158.7(1)	⟨∠Ni-O-Ni⟩		156.0(6)	156.2(5)	156.8(7)	157.1(6)
[*b*] tilt		11.4	11.3	11.0	10.8	[*b*] tilt		11.8	11.5	11.5	11.2
[*c*] tilt		11.1	11.1	10.7	10.7	[*c*] tilt		12.2	12.2	11.6	11.6
$d_{Ni\text{-}Ni}$	2	3.808(1)	3.811(1)	3.808(1)	3.818(1)	$d_{Ni\text{-}Ni}$	2	3.803(1)	3.804(1)	3.803(1)	3.805(1)
$d_{Ni\text{-}Ni}$	4	3.818(1)	3.817(1)	3.814(1)	3.813(1)	$d_{Ni\text{-}Ni}$	4	3.807(1)	3.808(1)	3.807(1)	3.808(1)

TABLE IV. Interatomic distances (Å) for rare-earth polyhedron and oxygen atoms. (Δ_d is defined as in Table III.)

	$PrNiO_3$					$NdNiO_3$			
		Temperature					Temperature		
	No.	1.5 K	110 K	145 K	RT	No.	1.5 K	170 K	215 K
$d_{Pr\text{-}O(1)}$	1	2.939(3)	2.929(3)	2.914(3)	2.896(4)	$d_{Nd\text{-}O(1)}$ (<4 Å)	1	2.974(4)	2.969(4)	2.963(6)
	1	2.509(3)	2.515(3)	2.521(3)	2.541(4)		1	2.480(4)	2.483(4)	2.476(6)
	1	3.064(3)	3.064(3)	3.051(4)	3.045(4)		1	3.063(9)	3.048(7)	3.071(9)
	1	2.370(3)	2.366(4)	2.375(4)	2.386(4)		1	2.343(9)	2.359(7)	2.339(9)
$d_{Pr\text{-}O(2)}$	2	2.580(2)	2.594(3)	2.590(3)	2.594(3)	$d_{Nd\text{-}O(2)}$ (<4 Å)	2	2.585(5)	2.580(4)	2.606(6)
	2	2.402(2)	2.404(3)	2.407(3)	2.407(3)		2	2.376(5)	2.372(4)	2.393(6)
	2	2.693(2)	2.684(3)	2.689(2)	2.700(2)		2	2.661(5)	2.671(4)	2.649(6)
$\langle d_{Pr\text{-}O} \rangle$		2.623(1)	2.624(1)	2.623(1)	2.627(1)	$\langle d_{Nd\text{-}O} \rangle$		2.611(2)	2.610(2)	2.615(2)
$10^4\Delta_d$		70.1	68.5	64.5	61.2	$10^4\Delta_d$		79.4	76.6	76.8
$d_{Pr\text{-}Ni}$	2	3.288(2)	3.293(3)	3.288(3)	3.292(3)	$d_{Nd\text{-}Ni}$	2	3.276(4)	3.272(4)	3.291(6)
	2	3.342(2)	3.337(3)	3.337(3)	3.342(3)		2	3.328(4)	3.332(4)	3.315(6)
	2	3.444(2)	3.442(2)	3.430(2)	3.424(3)		2	3.468(2)	3.464(2)	3.454(2)
	2	3.155(2)	3.157(2)	3.162(2)	3.173(2)		2	3.130(2)	3.135(2)	3.138(2)
$d_{O(1)\text{-}O(2)}$	2	2.748(2)	2.754(2)	2.745(2)	2.746(2)	$d_{O(1)\text{-}O(2)}$	2	2.755(7)	2.735(5)	2.756(7)
	2	2.738(2)	2.735(2)	2.734(2)	2.727(2)		2	2.730(6)	2.734(5)	2.733(7)
	2	2.759(2)	2.759(2)	2.754(2)	2.764(2)		2	2.762(5)	2.773(4)	2.743(6)
	2	2.752(2)	2.748(2)	2.743(2)	2.745(2)		2	2.755(5)	2.754(4)	2.753(6)
$d_{O(2)\text{-}O(2)}$	2	2.714(2)	2.715(2)	2.709(2)	2.710(2)	$d_{O(2)\text{-}O(2)}$	2	2.725(6)	2.721(5)	2.721(8)
	2	2.788(2)	2.785(2)	2.780(2)	2.784(2)		2	2.783(6)	2.786(5)	2.777(7)

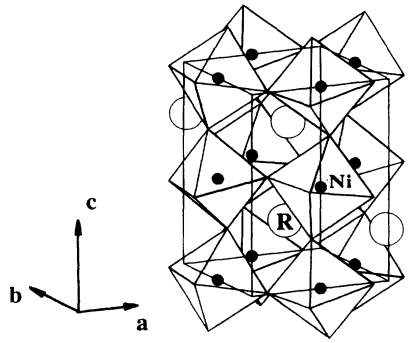

FIG. 1. Crystal structure of orthorhombic RNiO$_3$ showing the tilt of octahedra (see explanation in the text).

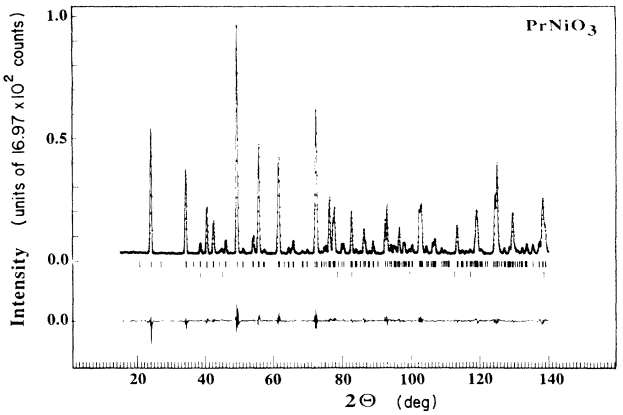

FIG. 2. Observed (+) and calculated (——) neutron-diffraction patterns (from D2B data) for PrNiO$_3$ at RT.

occupancy). This is an essential result for the discussion of the physical properties of these materials.

The main component of the distortion from the ideal cubic perovskite structure corresponds to the tilting of the NiO$_6$ octahedra, which is of the $a^0b^+c^+$ type. [In Glazer's terminology[19] the distortion is of $a^-b^-c^+$-pseudocubic type. For simplicity, we shall take the orthorhombic axes as reference. Hence $a^0b^+c^+$ means that tilts only occur around b or c orthorhombic axes. The positive signs mean that b and c tilts are in phase when successive octahedra along the same axis are considered (Fig. 1).] We define, up to first-order approximation, b and c tilts as follows: [b] tilt $\approx(180°-\alpha)/2$, [c] tilt $\approx(180°-\beta)/2$, where α and β angles are defined as $\alpha=\angle$Ni-O(1)-Ni and $\beta=\angle$Ni-O(2)-Ni. These angles are basic parameters in the magnetic and electronic behavior of these systems because they govern the transfer integral between Ni e_g and O $2p$ orbitals and, therefore, the electronic transfer and exchange energy among them. Their values, being about 20° away from the ideal 180° case, are presented in Table III.

Tilts are usually caused by the free space left in the structure, which is largely determined by the small size of R atoms and their positions in the $z=(2n+1)/4$ ab planes (n being integer). Thus, R displacements are accompanied by tilts of octahedra. Concerning the distortion of oxygen octahedra around the Ni atoms, Table III demonstrates that it is very small.

From the values in Table III, the average Ni-O distance in the Pr and Nd compounds [$\langle d_{\mathrm{NiO}}\rangle=1.942(1)$ Å] is very similar to that found by Demazeau *et al.*[8] in the insulator HoNiO$_3$ (1.94 Å). They reported flattened octahedra ($d_{\mathrm{Ni\text{-}O(1)}}=1.92$ Å, $d_{\mathrm{Ni\text{-}O(2)}}=1.94$ and 1.96 Å at RT) having ten times higher distortion, $\Delta_d=0.354\times10^{-4}$, than ours. From our data, octahedra are nearly perfect at this temperature. The more distorted octahedra found by Demazeau *et al.*[8] could be due to the low scattering power of O compared to Ho and Ni for x rays and, therefore, the lower reliability of the derived oxygen positions.

It is clearly apparent that, although quite similar, the octahedra tiltings are more important with Nd than they are with Pr, where the metallic state is more stable down to lower temperatures.

STRUCTURAL CHANGES AT THE *M-I* TRANSITION (R =Pr,Nd,Sm)

The high-resolution neutron study across the *M-I* transition has revealed subtle structural changes coinciding with the electronic localization. In addition, neutron-diffraction patterns showed the appearance of several very small reflections below 135 and 200 K for Pr and Nd compounds, respectively. We know, from a study with polarized neutrons,[20] that these small peaks are magnetic in origin. In the present work, we shall concentrate our analysis on the structural changes at the electronic transition.

The appearance of a gap at the Fermi level, probably between mixed oxygen $2p$ and e_g metal orbital states at the σ^* subbands, is of first order, as are the associated structural changes. Figures 3(a)–3(c) show the discontinuous volume change for all three compounds (R =Pr,Nd,Sm). Table V displays the volume expansion with respect to the volume on the metallic side, as well as the thermal expansion coefficients (α_V) just above and below the transition. In all three compounds, α_V becomes smaller in the semiconducting regime.

Figure 4 represents the thermal evolution of SmNiO$_3$ cell parameters compared with those of PrNiO$_3$ from D1B experiment.[11] These data have allowed us to calculate the three linear thermal expansion coefficients on both sides of the transition (cf. Table VI).

The angular range spanned by the D1B instrument only covered 11 nuclear reflections of NdNiO$_3$, and this small number was not enough to separate accurately the changes with temperature of the a and b parameters in this compound, due to its pseudocubic nature. This disadvantage was somewhat overcome by the use of the high-resolution diffractometer D2B, which covers a much wider angular range and works with a shorter wavelength. A total of 224 different nuclear Bragg reflections were included in the data analysis. Figure 5 shows the values obtained from D2B measurements on NdNiO$_3$.

Although they seem rather dramatic, it should be emphasized that the static structural changes revealed by neutrons and x rays are relatively small. Differences in

cell parameters and distances are always only a few thousandths of an Å.

In $PrNiO_3$ and $SmNiO_3$ the cell parameters undergo an abrupt change at the transition. The biggest changes (Table VI) occur in the c and b axes, whereas the a-axis jump is comparatively much smaller in both compounds. (It is interesting to remember that $a < b$ in $SmNiO_3$, whereas $a > b$ in $PrNiO_3$.) Although cell parameters ex-

TABLE V. Cell volume changes ($\Delta V/V$) at the M-I transition, and volume thermal expansion coefficients [$10^5\alpha_V$ (K^{-1})] in both regimes for $RNiO_3$ (R = Pr,Nd,Sm).

	$\Delta V/V$ (%)	α_V (semicond.)	α_V (metal)
$PrNiO_3$	0.25	0.56	1.57
$NdNiO_3$	0.23	1.37	2.30
$SmNiO_3$	0.15	1.63	2.87

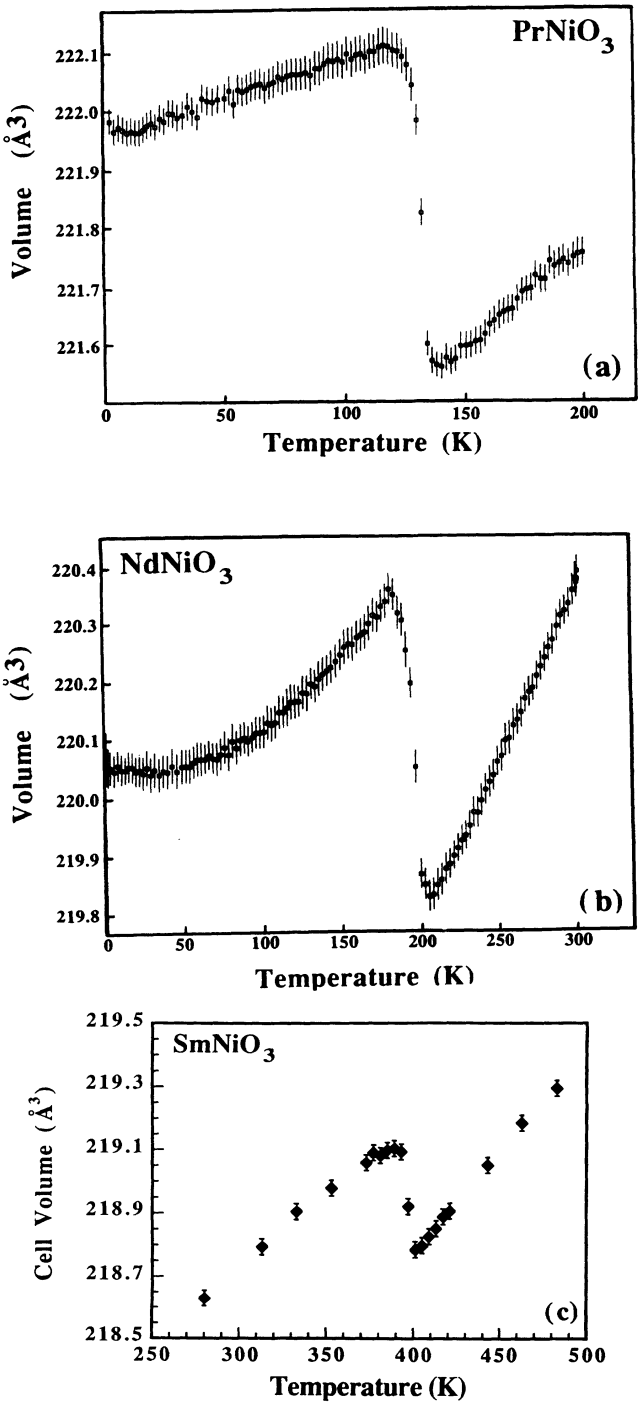

FIG. 3. Temperature dependence of volume of (a) $PrNiO_3$, (b) $NdNiO_3$ (neutron diffraction, instrument D1B, from Ref. 11), and (c) $SmNiO_3$ (x-ray diffraction, this work).

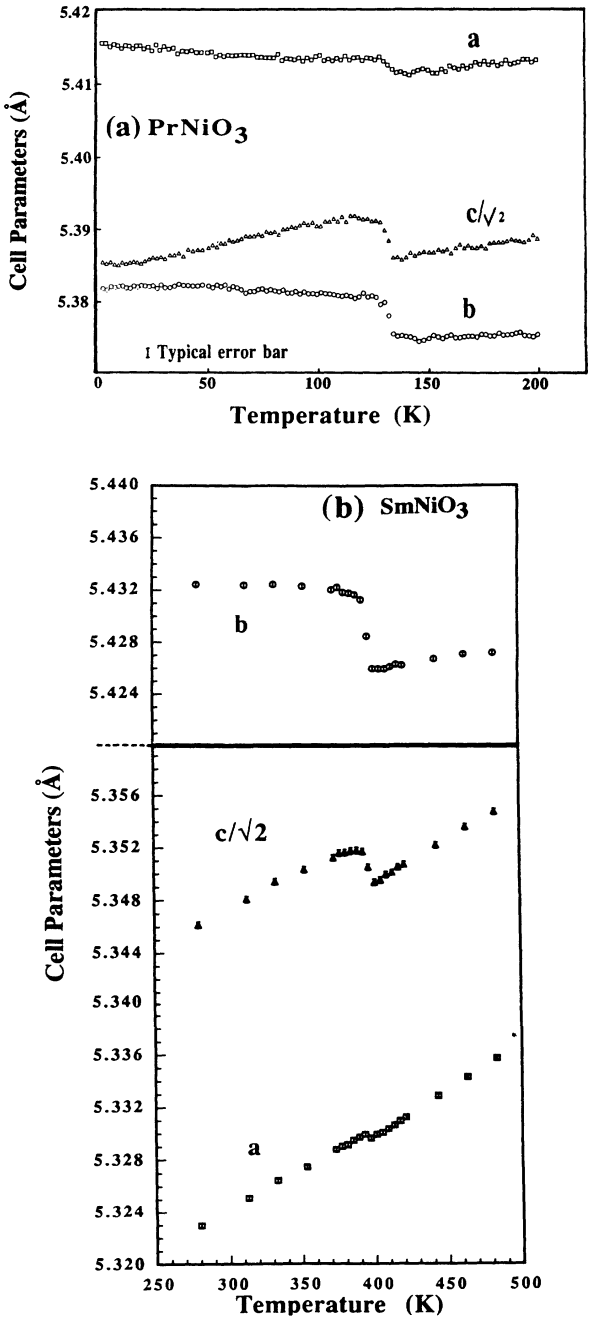

FIG. 4. Thermal evolution of (a) $PrNiO_3$ and (b) $SmNiO_3$ lattice constants showing the anomalous thermal expansion through the metal-insulator transition.

TABLE VI. Increment of cell parameters (%) and linear thermal expansion coefficients [$10^6\alpha_i$ (K^{-1})] through the transition for $PrNiO_3$ (neutron diffraction) and $SmNiO_3$ (x-ray diffraction) ($i=a,b,c$). (The estimated error for α_i is 10^{-6}.)

	Δi		α_i (semicond.)		α_i (metal)		$\Delta\alpha_i$	
	Pr (%)	Sm (%)	Pr	Sm	Pr	Sm	Pr	Sm
a	0.03	0.01	−0.3	11.2	5.4	13.4	5.6	2.2
b	0.12	0.11	−3.8	−0.4	1.1	3.0	4.9	3.4
c	0.10	0.05	10.7	10.0	8.3	12.5	−2.4	2.5

perience different thermal expansion depending on the compound and on the regime, it is to be noticed that, for both compounds, the *b* parameter exhibits the smallest overall thermal expansion, but the largest discontinuity at the transition. This also seems to be the case in $NdNiO_3$ (Fig. 5). Nevertheless, in this last compound, the *a* axis seems to decrease at the *M-I* transition, opposite to what happens in $PrNiO_3$ and $SmNiO_3$. However, any quick conclusion about an "anomaly" in $NdNiO_3$ must be viewed with caution because of the lower accuracy as a result of the cell pseudocubicity.

The lattice parameter variation is a manifestation of subtle changes in the structural arrangement. The results of our calculations for $PrNiO_3$ and $NdNiO_3$ are presented in Tables II–IV. Because of the low scattering power of oxygen for x rays, no reliable information could be obtained on the structural changes in $SmNiO_3$. The four sets of data for $PrNiO_3$ and $NdNiO_3$ were collected always from low to high temperatures to avoid hysteretic effects. Essentially, changes at the transition are (i) an increase in Ni-O distances, and (ii) a sudden increase in the tilts of octahedra.

The first important feature underlying the structural changes is the very slight (but significant) increase of Ni-O bond lengths, as is shown in Table III and Fig. 6. This small effect appears to be practically identical in both compounds. It should also be emphasized that it is of the same magnitude as the discontinuity in the unit-cell size.

The collective displacement of oxygen atoms, shown schematically in Fig. 7, corresponds to coupled tilts of octahedra in the sense of increasing rotation angles around the *b* and *c* axes. Therefore, the compounds always keep the $a^0b^+c^+$ symmetry and, within the margin of error imposed by resolution, the crystallographic structure in the insulator state down to 1.5 K is also well described in the *Pbnm* space group (see agreement factors in Table II), so that it appears that there is no change in symmetry across the *M-I* transition, only a small increment in the size of the unit cell. The tilting of octahedra at the transition is close to 0.5° for both $PrNiO_3$ and $NdNiO_3$ (see Table III and Fig. 8).

It is well known that, in a perovskite ABO_3, the tolerance factor[18]

$$t=d_{A\text{-}O}/d_{B\text{-}O}\sqrt{2}\ , \tag{1}$$

which is based on steric considerations, is a relevant parameter for estimating the degree of distortion of the cell when no other effects interfere. For instance, the orthorhombic distortion increases when *t* decreases. On the other hand, the $\Theta_{B\text{-}O\text{-}B}$ angle, which is a measure of the tilting of octahedra, is directly correlated to the cell distortion, Θ decreasing when the distortion increases. Therefore, *t* and Θ vary in the same way, and it is tempting to try to derive a correlation between these two parameters. In $PrNiO_3$ and $NdNiO_3$, the tolerance factors calculated with $d_{Ni\text{-}O}=1.940$ Å and $d_{R\text{-}O}$ as given for eightfold-coordinated rare-earth cations[21] are 0.9229 and 0.9171, and average Ni-O-Ni angles are 158.7° and 157.1°, respectively (see Table III). These values are close together, and a linear extrapolation between them should give a reasonable approximation of the correlation between small increments in tolerance factor and Ni-O-Ni angle, namely

$$\Delta\Theta\approx 275\Delta t^\circ\ . \tag{2}$$

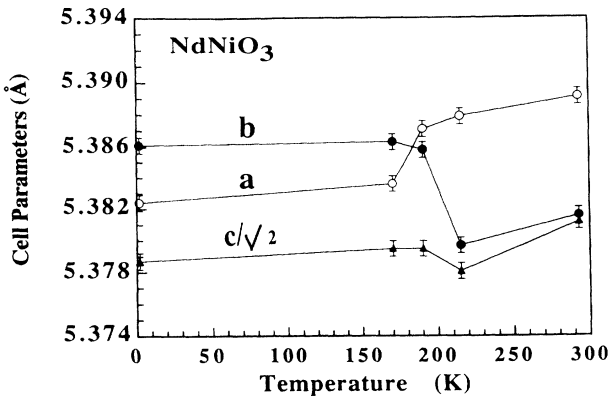

FIG. 5. Temperature dependence of $NdNiO_3$ cell parameters from D2B data.

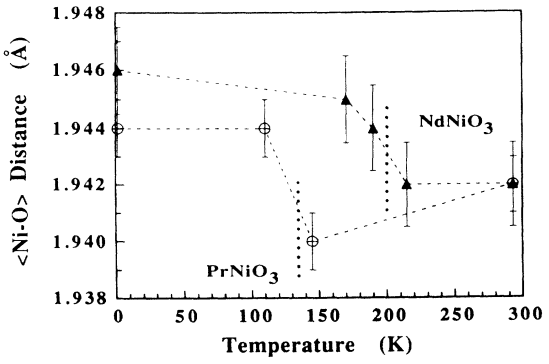

FIG. 6. Variation of $\langle d_{Ni\text{-}O}\rangle$ distance showing the effect of localization at the *M-I* transition. Bold dotted lines show the transition temperatures.

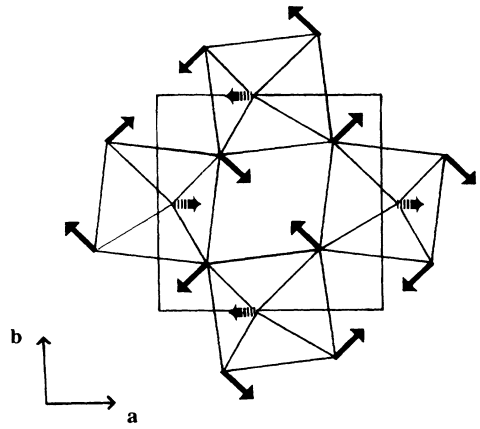

FIG. 7. xy projection of the NiO_6 coupled tilts around (010) and (001) axis that accompany the electronic localization upon cooling through the transition.

On the other hand, differentiating (1) gives the relationship between small increments in Ni-O distance and tolerance factor. Combining with (2) provides a simple relationship between small variations in $d_{\text{Ni-O}}$ and $\Theta_{\text{Ni-O-Ni}}$, when ruled by steric effects:

$$\Delta\Theta_{\text{Ni-O-Ni}} \approx -275(d_{R\text{-O}} d^2_{\text{Ni-O}} \sqrt{2})\Delta d_{\text{Ni-O}} \ .$$

When applied to the increment in Ni-O distance observed at the M-I transition in $PrNiO_3$ and $NdNiO_3$ (the average apparent jump is $\Delta d_{\text{Ni-O}} \approx 0.0035$ Å), it gives an approximation to what should be the variation of the average Ni-O-Ni angle if steric effects predominate, namely $\Delta\Theta_{\text{Ni-O-Ni}} \approx -0.46°$. This is the same sign and order of magnitude as $\Delta\Theta$ measured in these compounds at the transition (see Fig. 8 and Table III). It is a strong indication that oxygen displacements upon decreasing temperature through the transition are merely a regular accommodation of the perovskite framework to the abrupt slight enhancement of the Ni-O distance, which itself is triggered by the electronic localization. The fact that the structure keeps the $Pbnm$ symmetry through the transition confirms that no parasitic effects interfere. The driving physical phenomenon would thus be the sudden electronic localization, the structural framework sterically reacting in order to compensate for the increased Ni-O distance.

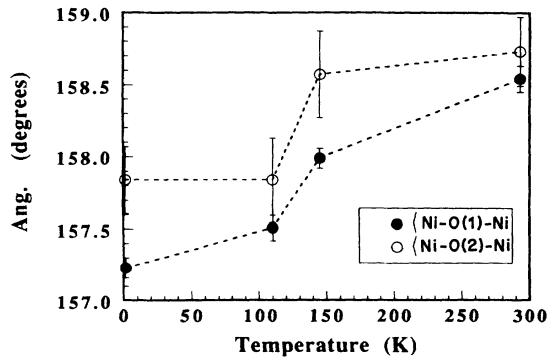

FIG. 8. Jump at the M-I transition, in $PrNiO_3$, of the superexchange Ni-O-Ni angles, which govern the transfer integral between Ni $3d$ and O $2p$ orbitals.

EFFECTIVE d STATE OF Ni AND BOND VALENCE CALCULATIONS

An important point to be considered in the $RNiO_3$ series concerns the electronic structure of the Ni ions. As pointed out above in the Introduction, doping (or nonstoichiometry) creates holes in the oxygen p band (O^-) in several nickel and copper oxides.[12–14] However there is no general agreement about systems such as $LiNiO_2$ or $LaCuO_3$, where the electronic state of the TM cations is still very controversial. Thus, in our case there may be reasonable doubts about the primary character of created holes in $RNiO_3$ when the system is seen as oxygen-doped $RNiO_{2.5}$ ($R^{3+}Ni^{2+}O^{2-}{}_{2.5}$), that is, about the effective d state of Ni in these systems. To tackle this problem, it is evident that a spectroscopic technique directly probing electronic configurations would be desirable, and such a study has been undertaken using x-ray absorption near K shells of nickel and oxygen.

The results of the crystallographic analysis by high-resolution powder diffraction provide an empirical way to say something about the problem of "formal" valences of the different ions in $RNiO_3$. The approach followed in this section is a chemical one: the valence-bond method (VBM) as described by Brown[22] or O'Keeffe[23] is a powerful and simple procedure for obtaining an insight into the valence from the observed bond lengths.[24]

All the calculations have been done at room temperature, where the R_0 parameters are known.[24] The compounds are metallic, but VBM is not sensitive enough to discriminate their metallic or insulator nature. This may be an indication of a low number of carriers per Ni atom. The calculations using the room-temperature values of R_0 with the data at low temperature give essentially the same relative results, with only a small increase in all formal valences.

If we assume R^{3+} and O^{2-}, the calculated valance of R cations, using the standard values for R_0, must give a value very near to 3. This assumption (Table VII) seems quite correct because, even in the metallic state, it gives a maximum discrepancy of about 2.1%. If we consider that $RNiO_3$ can be treated as an oxygen (hole) -doped $R^{3+}Ni^{2+}O^{2-}{}_{2.5}$, and holes are localized (at least in the insulator state) on oxygen atoms, the chemical formula in the ionic limit could be written as $R^{3+}Ni^{2+}O^{2-}{}_2O^{1-}$. In that case there must be two crystallographic positions for oxygen, with a ratio of multiplicities equal to 2. This is actually the case for orthorhombic $RNiO_3$. However, the difference between the distances $d_{\text{Ni-O(1)}}$ and $d_{\text{Ni-O(2)}}$ is too small (<0.01 Å) in all cases to believe in a "selective" hole localization. If one is convinced (as is the Sawatzky's team[12–14]) that the electronic structure of hole-doped Ni oxides is better described by states of the form $d^8\underline{L}$, one has to consider that "holes" in $RNiO_3$ must be "shared" by all the oxygens even in the insulator state. That gives rise to a formal valence of $\frac{5}{3} = 1.667$ for

TABLE VII. Average cation-anion distances ($\langle R \rangle$) in Å, coordination numbers (N), valence sums (V), and deviation from the valence-sum rule (expected charge) [$\delta V(\%)=100(V-Q)/Q$]. The R_0 constant for the Ni^{III}-O^{2-} pair was taken from Ref. 25 ($R_0=1.68$) and the predicted average distance is 1.937 Å.

	(a) $LaNiO_3$ (RT)		
	La	Ni	O
$\langle R \rangle$	2.719(1)	1.935(1)	
N	12	6	6
V	3.05(1)	3.01(1)	2.02(1)
δV (%)	1.6	0.4	1.0

	(b) $PrNiO_3$ (RT)			
	Pr	Ni	O(1)	O(2)
$\langle R \rangle$	2.581(1)	1.942(1)		
N	9	6	5	5
V	2.94(1)	2.96(1)	1.96(1)	1.97(1)
δV (%)	2.0	1.4	2.1	1.5

	(c) $NdNiO_3$ (RT)			
	Nd	Ni	O(1)	O(2)
$\langle R \rangle$	2.567(2)	1.942(1)		
N	9	6	5	5
V	2.95(2)	2.95(1)	1.97(1)	1.97(1)
δV (%)	1.6	1.5	1.5	1.6

oxygen. The predicted average distance, from $R_0=1.654$,[25] for a Ni^{2+}-O^{2-} bond is 2.06 Å in an octahedrally coordinated Ni^{2+}, which is obviously too high compared with the average distance $d_{Ni\text{-}O}=1.942$ Å observed for $RNiO_3$. In the hypothesis of shared holes we can deduce the R_0 value for the Ni^{2+}-$O^{1.67-}$ bond from the observed distance. This value ($R_0=1.685$ Å) is very similar to the $R_0(Ni^{III}\text{-}O^{2-})=1.68$ derived in Ref. 25. If the hypothesis Ni^{2+}-$O^{1.67-}$ is retained, it is necessary to suppose that $R_0(R^{3+}\text{-}O^{2-})=R_0(R^{3+}\text{-}O^{1.67-})$, which seems unphysical.

The VBM calculations suggest that the classical valence states R^{3+}, Ni^{III} (low spin), and O^{2-} are a good first approximation to the electronic structure in this system. The summary of VBM calculations is given in Table VII with R_0 parameters taken from Ref. 25. The conclusion is that $RNiO_3$ cannot be considered as an "oxygen-localized-holes" compound as Li-doped NiO seems to be. Magnetic data[20] have been found to be consistent with this conclusion.

CONCLUSIONS

These results should be analyzed in the light of what is known about the extreme compound of the series, $LaNiO_3$, that is, metallic behavior with highly correlated conduction electrons of large effective mass ($m \approx 6m_e$) and a low density of states near E_F [0.5–1.0 state/eV per unit cell is the value expected from a band calculation,[10] whereas photoelectron spectroscopy gives $n(E_F)=0.1$ state/eV per unit cell]. This indicates that, probably, hybridization between the TM $3d$ and oxygen $2p$ orbitals

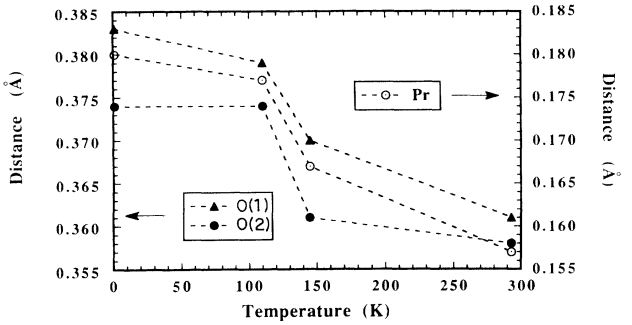

FIG. 9. In $PrNiO_3$, atomic shifts in Å from the ideal cubic perovskite atomic positions as a function of temperature.

(T_{pd}) determines a dispersional conduction-band width (W) very close to the critical value imposed by the charge-transfer excitations energy (Δ, assuming, according to Ref. 7, their location at the boundary between the metallic and the charge-transfer insulating regions). This picture is highly supported by the discovery[11] of the metal-insulator transition in $PrNiO_3$, $NdNiO_3$, and $SmNiO_3$, whose critical temperature rises systematically with the closing of the Ni-O-Ni angles and, therefore, with the covalence T_{pd} parameter. However, no simple relationship has been found yet between the absolute values of $T_{M\text{-}I}$ and those of the relevant simple structural parameters analyzed in this work.

At the present stage, it is very difficult to infer the real origin of the electronic transition. Further experimental work and a detailed knowledge of the electronic structure are needed. The described slight structural changes, which are electronically driven and keep the *Pbnm* symmetry, are only one aspect of the physics involved.

In Fig. 9 atomic shifts, in Å, from the ideal perovskite positions for $PrNiO_3$ are represented as a function of temperature. As temperature is lowered, atoms are displaced more and more from the ideal positions, which implies a systematic closing of Ni-O-Ni exchange angles and variations of the Ni-O covalence and probably of conduction-band width. High-resolution x-ray-absorption studies are necessary to get into the details of the changes in the electronic structure leading to the enhancement of the nickel to oxygen bond lengths below $T_{M\text{-}I}$, which is responsible for the structural anomalies described in this work.

In summary, in addition to the structural description, valence-bond calculations of the high-resolution data (consistent with the magnetic behavior[20]) suggest that the electronic state of nickel in $RNiO_3$ is most probably low-spin Ni^{III}. These results are in contrast with the presence of oxygen holes reported for other nickel oxides such as $Li_xNi_{1-x}O$ and $La_{2-x}Sr_xNiO_4$.[13]

ACKNOWLEDGMENTS

The authors express their thanks to Dr. R. Retoux for having performed the high-temperature x-ray thermodiffractometry on $SmNiO_3$. The Laboratoire des Fluorures is "Unité Associée au Centre National de la Recherche Scientifique No. 449."

[1]F. Bloch, Z. Phys. **57**, 545 (1929).
[2]A. H. Wilson, Proc. R. Soc. London Ser. A **133**, 458 (1931).
[3]N. F. Mott, Proc. Phys. Soc. London Sec. A **62**, 416 (1949).
[4]J. Hubbard, Proc. R. Soc. London Ser. A **277**, 237 (1964); **277**, 401 (1964).
[5]D. B. McWhan, J. P. Remeika, T. M. Rice, W. F. Brinkman, J. Maita, and A. Menth, Phys. Rev. Lett. **27**, 941 (1971); Phys. Rev. B **5**, 2252 (1972).
[6]J. Zaanen, G. A. Sawatzky, and J. W. Allen, Phys. Rev. Lett. **55**, 418 (1985).
[7]J. B. Torrance, P. Lacorre, C. Asavaroengchai, and R. M. Metzger, J. Solid State Chem. **90**, 168 (1991).
[8]G. Demazeau, A. Marbeuf, M. Pouchard, and P. Hagenmuller, J. Solid State Chem. **3**, 582 (1971).
[9]J. B. Goodenough, N. F. Mott, M. Pouchard, G. Demazeau, and P. Hagenmuller, Mater. Res. Bull. **8**, 647 (1973).
[10]J. P. Kemp and P. A. Cox, Solid State Commun. **75**, 731 (1990).
[11]P. Lacorre, J. B. Torrance, J. Pannetier, A. I. Nazzal, P. W. Wang, T. C. Huang, and R. L. Siemens, J. Solid State Chem. **91**, 225 (1991).
[12]Jan van Elp, Ph.D. thesis, University of Groningen, The Netherlands, 1991, Chap. 1.
[13]P. Kuiper, G. Kruizinga, J. Ghijsen, and G. A. Sawatzky, Phys. Rev. Lett. **62**, 221 (1989).
[14]P. Kuiper, G. Kruizinga, J. Ghijsen, M. Grioni *et al.*, Phys. Rev. B **38**, 6483 (1988).
[15]J. Rodríguez, M. Anne, and J. Pannetier (unpublished).
[16]A. Wold, B. Post, and E. Banks, J. Am. Chem. Soc. **79**, 4911 (1957).
[17]T. C. Huang, W. Parrish, H. Toraya, P. Lacorre, and J. B. Torrance, Mat. Res. Bull. **25**, 1091 (1990).
[18]J. B. Goodenough and J. M. Longo, in *Magnetic and Other Properties in Oxides and Related Compounds,* edited by K. H. Hellwege and A. M. Hellwege, Landolt-Börnstein, New Series, Group III, Vol. 4a (Springer-Verlag, Berlin, 1970), Chap. 3, p. 126.
[19]A. M. Glazer, Acta Crystallogr. Sec. A **31**, 756 (1975).
[20]J. L. García-Muñoz, J. Rodríguez-Carvajal, and P. Lacorre (unpublished).
[21]P. Poix, C. R. Acad. Sci. Ser. C **270**, 1852 (1970).
[22]I. D. Brown, in *Struct. Bonding in Crystals,* edited by M. O'Keeffe and A. Navrotsky (Academic, New York, 1981), Vol. 2, pp. 1–30.
[23]M. O'Keeffe, Struct. Bonding (Berlin) **71**, 162 (1989).
[24]The VBM is based on the empirical relationship between the bond length and the valence of the bond: $s_{ij}=\exp[(R_0-d_{ij})/B]$, where R_0 is a constant characteristic of the cation-anion pair, and $B=0.37$ Å is a "universal" constant. The valence-sum rule (VSR), $V_i=\sum s_{ij}$, states that the sum of valence bonds around a cation (anion) must be equal to the formal charge of the cation (anion). The VSR is verified, within a few percent, for all inorganic compounds having crystal structures with enough degrees of freedom (e.g., atoms in general positions). In those cases and when two kinds of cations coexist in the structure, it would be possible to test different assumptions about formal charges and select one of them because the assumed charge for the anion must satisfy the VSR for the two kind of cations. The case of $RNiO_3$ clearly belongs to this class of structures.
[25]N. E. Brese and M. O'Keeffe, Acta Crystallogr. Sec. B **47**, 192 (1991).